JOURNAL OF THERMOPHYSICS AND HEAT TRANSFER
Vol. 31, No. 2, April–June 2017

Influence of Thermal Sensor Installation on Measuring Accuracy at Stagnation Points

Qiu Wang,* Jin-Ping Li,† Wei Zhao,‡ and Zong-Lin Jiang§
State Key Laboratory of High-Temperature Gas Dynamics, Institute of Mechanics, Chinese Academy of Sciences, 100190 Beijing, People's Republic of China

DOI: 10.2514/1.T4971

The development of suitable heat-resistant material and reasonable thermal structure design for a hypersonic aircraft requires highly precise heat transfer prediction, especially at the wing tips or stagnation points where the thermal environment is particularly rigorous. Unfortunately, existing techniques for measuring heat flux via thermal sensors in hypersonic test facilities are excessively complex; any slight deviation from ideal conditions may lead to inaccuracy. In this study, the influence of installation on the accuracy of heat flux measurement for a sphere model using cylindrical thermal sensors was numerically investigated. The sensors examined were protruding or recessed from the model surface on the order of 0.1–0.5 mm, and the influence of variations in installation was estimated by comparing the results against the smoothly installed sensor. Experiments were also run using different Reynolds numbers and sensor diameters to ensure the rules and mechanisms reported are as comprehensive as possible. Results showed that "unsmooth" (i.e., protruding, recessed) installation creates substantial deviation from the actual heat transfer rate; protruding installation resulted in larger deviation than recessed, and the deviation of either installation configuration grew more severe at larger depths from the model surface.

Nomenclature

D	=	thermal sensor diameter, mm
k	=	thermal conductivity coefficient, W/(m · K)
L	=	depth of sensor surface from the model vertex, mm
P	=	pressure, Pa
q	=	heat flux rate, MW/m^2
R	=	sphere radius, mm
Re	=	freestream unit Reynolds number, 1/m
T	=	temperature, K
u	=	velocity, m/s
δ	=	boundary-layer thickness, m

Subscripts

e	=	boundary-layer edge
w	=	sphere wall
∞	=	freestream flow

I. Introduction

HYPERSONIC technology represents one of the most important issues affecting the future of the aerospace industry. Hypersonic flight is characterized by high speed, shock compression, and viscous energy dissipation behind the bow shock of an aircraft leading edge, all of which occurs at very high temperature. A massive amount of kinetic energy is then converted into heat energy, which makes the thermal environment become severe, especially at wing-tip or stagnation point regions. To this effect, accurately predicting heat transfer rates is a major issue for researchers and developers working within the current space program [1].

Because of the high cost of flight tests, most aerodynamic heating experiments are performed in ground impulse facilities, such as shock tubes and shock tunnels, which can simulate the required aerothermal environment at low cost of operation. Heat flux sensors, typically in cylindrical shape with diameter from 1 to 2 mm, are primarily used for heat transfer measurement in these facilities [2]. In general, the local convective heat transfer rate is greatest at the stagnation point, which is downstream of the normal portion of the bow shock wave. The same point is often considered the denominator in nondimensional correlations of convective heat transfer distributions. Considerable attention is often given, as such, to defining the flowfield in the stagnation region. Heat transfer measurement techniques have been extensively studied throughout recent decades, however, they remain largely elusive due to excessive complexity; existing techniques have yet to be sufficiently improved with respect to measurement accuracy and repeatability. There is, of course, a tremendous amount of literature pertaining to this subject, from experimental techniques to analytical and computational analyses [3–6]. Heat flux is usually determined based on the measured temperature development on the surface or inside the probe and then applying a mathematical model with a few (mostly simplification) assumptions; unfortunately, the measurement is so complicated that any deviation from a perfect contact between the temperature sensor and probe (or any other even minor issue with the assumptions, such as transverse heat transfer) leads to inaccuracy.

Any improvements in heat transfer measurement techniques necessitate in-depth investigation of the technique, including gauge installation, gauge calibration and sensitivity tests, data reduction procedures, and analysis of gauge diameter effects and uncertainty [7]. Zeng et al. [8] studied the error mechanism of stagnation points in the shock tunnel via numerical simulation to investigate changes in the flowfield and wall heat transfer caused by variations in stagnation region curvature due to the installation of sensors, ultimately establishing a useful correction method and corresponding coefficient. In another interesting study, Coblish et al. [9] examined the influence of material thermal properties on heat transfer measurement for coaxial thermocouple sensors and made valuable suggestions for further investigation to improve accuracy.

Although there has been progress in improving the accuracy of heat transfer measurements in recent decades, there is still a difference of ±10% between experimental and theoretical results for the standard model [1]; the difference is even greater at certain local

Received 4 April 2016; revision received 21 June 2016; accepted for publication 16 August 2016; published online 23 November 2016.

*Assistant Professor, Institute of Mechanics, No. 15 Beisihuanxi Road; wangqiu@imech.ac.cn.

†Associate Professor, Institute of Mechanics, No. 15 Beisihuanxi Road; lijinping@imech.ac.cn (Corresponding Author).

‡Professor, Institute of Mechanics, No. 15 Beisihuanxi Road; zw@imech.ac.cn.

§Professor, Institute of Mechanics, No. 15 Beisihuanxi Road; zljiang@imech.ac.cn. Associate Fellow AIAA.

regions of a complex model. It remains necessary to extensively investigate the factors and rules influencing heat transfer measurements before further progress can be made.

In such experiments, it is expected that the sensors have been installed with absolute smooth transition with the test model, and that local surface curvature is not affected. In actuality, however, the sensors are installed more or less protruding or recessed with the model surface, though at very small (and easily overlooked) scale. When typical thermal sensors are installed protruding with the model surface, it is possible to create a better coaxial thermocouple by mechanical sanding; this cannot be done for thin-film resistors or calorimeters, though, due to technological limitations. It is not possible to improve recessed conditions apart from smoothly reinstalling the thermal sensors entirely. In any case, nonideal sensor installation effects inextricably exist, substantially affect heat transfer measurement accuracy, and have yet to be very extensively researched.

In view of the importance and representativeness of stagnation point heat transfer, the primary goal of the present study was to examine the influence of installation on its accuracy under different flow conditions. We examined cases in which sensors were protruding or recessed from the model surface on the order of 0.1–0.5 mm (though each may be smaller during actual installation). We investigated the related rules and mechanism accordingly in an effort to provide theoretical guidance for the design and error analysis of aerodynamic heating experiments.

II. Physical Problems

We noticed a pattern after analyzing a few unusual measuring points in the previous aerodynamic heating experiment on a sharp cone, where the results deviated from the theoretical value by more than 10%; this experiment was conducted with the model scale and test conditions found in the literature [1]. The most notable cause of said deviation was the unsmooth installation of the thermal sensors; the measured heat flux rate was consistently greater than the theoretical value when the sensors were installed protruding with the model surface, and consistently smaller under recessed conditions, even when the degree to which the sensors were installed as either protruding or recessed was very small. We designed our experiment to address these issues using rear-mounted sensors on the model shown in Fig. 1. Three 1.4-mm-diam coaxial thermocouples were installed differently for the sake of comparison: The central thermocouple was installed as smoothly as possible, and the other two were installed protruding and recessed from the model surface on the order of about 0.2 mm (i.e., too small to be precisely measured with a Vernier caliper). The temperature rising curves of the three sensors are shown in Fig. 2, where there is a clear difference between the smoothly installed sensor and the other two; protruding installation resulted in a higher temperature rising curve and recessed installation in a lower rising curve.

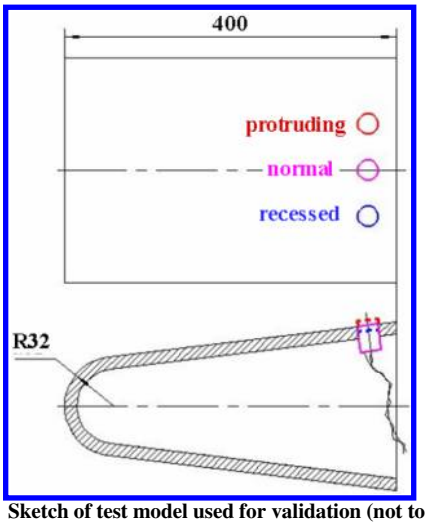

Fig. 1 Sketch of test model used for validation (not to scale).

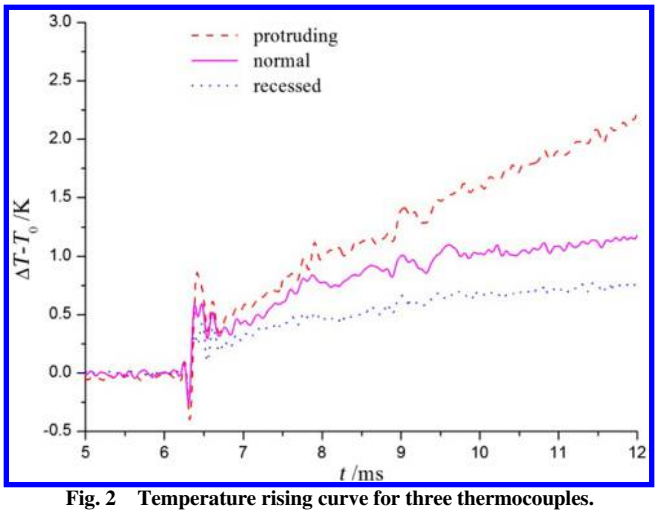

Fig. 2 Temperature rising curve for three thermocouples.

In a word, the results showed that unsmooth installation of the thermal sensor sizably affected heat transfer measurement accuracy. We plan to conduct a series of follow-up experiments to further explore this phenomenon in the future, but for the purposes of the present study, we went on to explore these observations using a numerical method for its easier operation and better understanding provided.

Considering the importance of stagnation point heat transfer in aerodynamic heating (as mentioned earlier, the stagnation point is often used as the denominator in nondimensional correlations), we used the sphere model (but not the test region) shown in Fig. 1 for analysis. To reduce the influence of sensor installation on the surface curvature, we used a slightly large sphere (30 mm in diameter) to account for the fact that typical thermal sensors are less than 2 mm in diameter. A sketch of the computing model is shown in Fig. 3, where D is the sensor diameter, L is the depth (either protruding or recessed) from the model vertex, and R is the sphere radius. Three sensor diameters were tested: 1.4, 1.7, and 2 mm. (Notably, 1.4 mm conditions are the main research objects for the wide application of coaxial thermocouples in the authors' laboratory.) In general, as discussed earlier, the degree to which a manually installed sensor deviates from the ideal installation is usually very slight (or else it is reinstalled). To fully elucidate the relevant rules and mechanism, L was set to 0, 0.1, 0.2, 0.3, and 0.5 mm in each case, though some values may potentially be greater than in actual situations. L equal to 0 mm represented a smoothly installed sensor condition.

Detailed calculation conditions and the freestream flows are described in Table 1, where cases 1 and 2 are the typical test conditions of the JF12 shock tunnel in the authors' institute. Freestream flows were selected by taking into consideration the effect

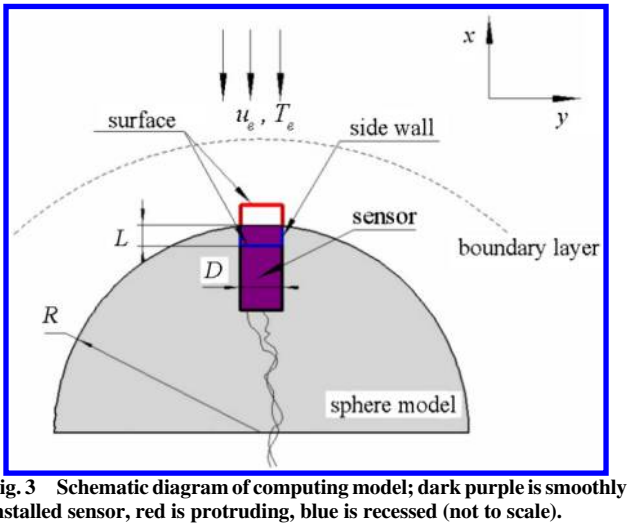

Fig. 3 Schematic diagram of computing model; dark purple is smoothly installed sensor, red is protruding, blue is recessed (not to scale).

Table 1 Calculation parameters and heat flux rates of $R = 15$ mm sphere model

Case	P_∞, Pa	T_∞, K	Re, /m	D, mm	q_0, MW/m^2 CFD	q_0, MW/m^2 Fay and Riddell [14]
1	390	324	0.5×10^6	1.4	1.47	1.38
2	394	221	0.9×10^6	1.4	1.03	0.97
3	575	236.5	1.2×10^6	1.4, 1.7, 2	1.31	1.23
4	5750	236.5	12×10^6	1.4	4.15	3.89

of Reynolds number, an important parameter for heat transfer analysis. It is also worth mentioning that the heat transfer rate in our case was the average heat flux within half of the sensor diameter on the surface, because the sensitive element of a thermal sensor is usually placed nearby.

III. Simulation Methodology

The following governing equations were employed, including axisymmetric, compressible Navier–Stokes equations assuming laminar flow:

$$\frac{\partial U}{\partial t} + \frac{\partial F}{\partial x} + \frac{\partial G}{\partial y} + H = \frac{\partial F_v}{\partial x} + \frac{\partial G_v}{\partial y} + H_v \tag{1}$$

$$U = \begin{bmatrix} \rho \\ \rho u \\ \rho v \\ E \end{bmatrix}, F = \begin{bmatrix} \rho u \\ \rho u^2 + p \\ \rho uv \\ u(E+p) \end{bmatrix}, G = \begin{bmatrix} \rho v \\ \rho uv \\ \rho v^2 + p \\ v(E+p) \end{bmatrix}$$

$$, H = \frac{1}{y}\begin{bmatrix} \rho v \\ \rho uv \\ \rho v^2 \\ v(E+p) \end{bmatrix}, F_v = \begin{bmatrix} 0 \\ \tau_{xx} \\ \tau_{xy} \\ u\tau_{xx} + v\tau_{xy} + q_x \end{bmatrix},$$

$$G_v = \begin{bmatrix} 0 \\ \tau_{xy} \\ \tau_{yy} \\ u\tau_{xy} + v\tau_{yy} + q_y \end{bmatrix}, H_v = \frac{1}{y}\begin{bmatrix} 0 \\ \tau_{xy} \\ \tau_{yy} - \tau_{\theta\theta} \\ u\tau_{xy} + v\tau_{yy} + q_y \end{bmatrix} \tag{2}$$

where x and y are the axial and radial coordinates of the physical space; U is the conservative variable vector; F, G, and H are the inviscid flux vectors; F_v, G_v, and H_v are the viscous flux vectors, respectively; and ρ, u, and E are density, velocity, and total energy per unit volume. The shear stress, heat flux, and state equations are given by Eqs. (3–5), namely,

$$\tau_{xx} = \frac{2}{3}\mu\left(2\frac{\partial u}{\partial x} - \frac{\partial v}{\partial y}\right), \quad \tau_{yy} = \frac{2}{3}\mu\left(2\frac{\partial v}{\partial y} - \frac{\partial u}{\partial x}\right),$$
$$\tau_{xy} = \mu\left(\frac{\partial u}{\partial y} + \frac{\partial v}{\partial x}\right) \tag{3}$$

$$q_x = -k\frac{\partial T}{\partial x}, \quad q_y = -k\frac{\partial T}{\partial y} \tag{4}$$

$$\rho E = \frac{p}{\gamma - 1} + \rho\frac{u^2 + v^2}{2}, \quad p = \rho RT \tag{5}$$

The coefficient of μ in Eq. (3) is computed by the Sutherland formula, whereas the thermal conductivity coefficient k is derived from the Prandtl number. The definition of other variables can be found in the literature [10].

Considering the axial symmetry of the computing model in Fig. 3, half of the geometries have been calculated in the present study. The geometries with a recessed sensor installation at the nose of the sphere were discretized into two blocks, structured grids, as shown in Fig. 4. The mesh sizes of 160×360 and 200×161 were applied to block one and two, respectively, with 160 and 200 grid nodes across the axial coordinates. The zones near the sensor surface (i.e., block two) were incorporated with clustered points. The grid spacing in the streamwise direction was 2.5×10^{-6} m at recessed conditions of $L = 0.5$ mm, where the cell Reynolds number is about 13, and both of them are much less in other cases. The protruding conditions had similar treatment on the grids.

The governing equations were solved using a finite difference approach; convective terms were approximated using the AUSMPW+ [11,12] scheme and the central difference method was applied to the viscous terms. Time integration was performed implicitly by applying the lower-upper symmetric Gauss–Seidel algorithm [13]. No-slip and isothermal boundary conditions were specified as the boundary conditions at the wall, and temperature was set to 290 K.

IV. Results and Discussion

The convective heat transfer rate q_w along the model surface was calculated according to $q_w = k(\partial T/\partial n)_w$, where k is the thermal conductivity coefficient and T is temperature. The subscript n denotes the normal derivative at the model surface and w denotes the wall. Comparison between computational fluid dynamics (CFD) and theoretical data of an $R = 15$ mm sphere model at the stagnation point is shown in Table 1, with the latter obtained through the equation provided by Fay and Riddell [14]. Taking into account the complexity of simulation for aerodynamic heating [15], it is acceptable that the calculation was within 7% dispersion of the theoretical value.

The results of our analysis of the influence of sensor installation on heat transfer measurement are displayed using the nondimensional form of q_w/q_0, where heat transfer rate q_0 represents the smoothly installed condition (i.e., $L = 0$ mm). Please note that q_w or q_0 as discussed here apply only to the stagnation point. Results for q_w/q_0 that are greater than one indicate larger measuring results, and below one smaller; q_w/q_0 closer to one accordingly indicates smaller influence on measurement results, and vice versa farther from one.

Figure 5 shows the heat transfer rates for sensors installed either protruding or recessed from the model surface, where D is 1.4 mm and L varies from 0.1 to 0.5 mm (case 3). As shown in the figure, protruding installation led to larger deviation and recessed to smaller deviation from the actual measurements, in accordance with the

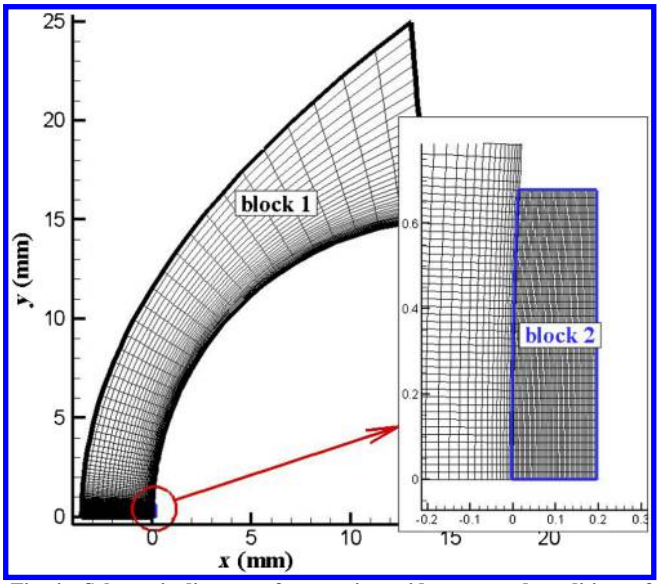

Fig. 4 Schematic diagram of computing grid at recessed conditions of $L = 0.2$ mm (a quarter of the grid density displayed).

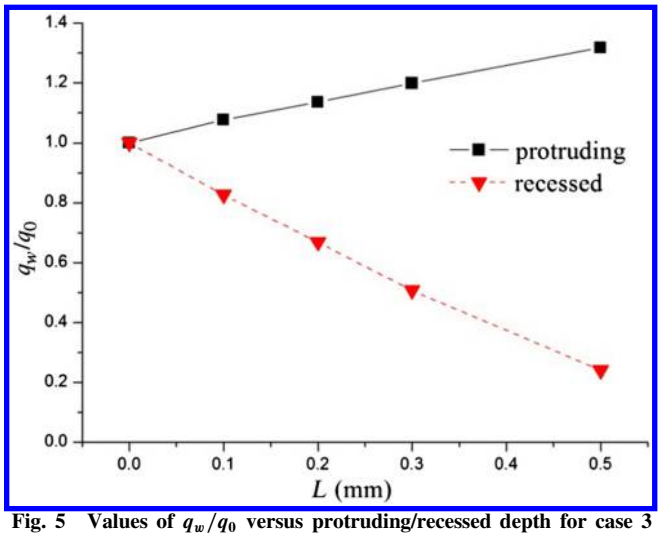

Fig. 5 Values of q_w/q_0 versus protruding/recessed depth for case 3 ($D = 1.4$ mm).

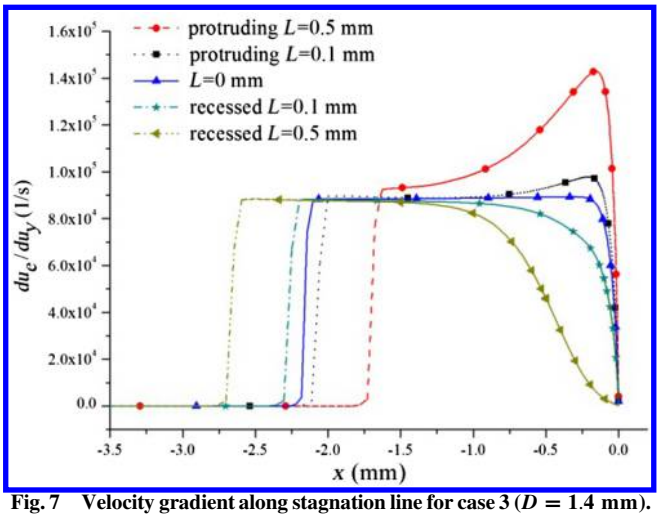

Fig. 7 Velocity gradient along stagnation line for case 3 ($D = 1.4$ mm).

experiments discussed earlier. Further, the value of q_w/q_0 was proportional to L, that is, the deeper the protruding or recessed depth, the larger the effect on the heat transfer measurement accuracy. To better understand the causes of these phenomena, we examined the temperature field and streamline around the sensors, as shown in Fig. 6. We found that the gas relieved outward when encountering the sphere, as shown in Fig. 6a, and to a greater degree in protruding conditions due to the protruding step shown in Fig. 6b; the gas was blocked by the recessed cavity as shown in Fig. 6c.

The observed gas flow enhancements/blockages were then quantitatively analyzed according to the velocity gradient along the stagnation line (Fig. 7), where $q_w \propto \sqrt{(\mathrm{d}u_e/\mathrm{d}y)}$ for the stagnation point and the subscript e denotes the edge of the boundary layer. As seen in Fig. 7, protruding installation created a larger velocity gradient, especially at greater depths, compared with the smoothly installed sensor; the opposite was true of recessed installation. Boundary-layer thickness δ was affected as a result of the effects on gas flow: It was smaller under protruding conditions and larger under recessed conditions. In turn, the temperature gradient at the wall $(\partial T/\partial x)_w$, which was $\mathcal{O}(T_e/\delta)$, was also affected; because $q_w = k(\partial T/\partial x)_w$, the heat flux rate was influenced significantly by both types of unsmooth installation.

Figure 5 also shows a comparison of q_w/q_0 between protruding and recessed conditions, further confirming that recessed sensor installation had greater effect on heat transfer measurement accuracy than protruding. At recessed depth of 0.1 mm, measurement results were smaller by about 18%, and by 76% when depth increased to 0.5 mm; the results were greater by about 8 and 32%, respectively, for the same protruding depths. These observations suggest that thermal sensors should, of course, be installed as smoothly as possible with the model surface whenever high-accuracy heat transfer measurement is desired; special attention must be given to prevent recessed installation to prevent particularly severe deviation.

The Reynolds number is an important parameter to consider when addressing aerodynamic heating problems. Figures 8a and 8b show the influence of the Reynolds number on q_w/q_0 under both protruding and recessed conditions with Re from 0.5×10^6 to 12×10^6/m and D equal to 1.4 mm. As shown in Fig. 8a, the effect of protruding installation on heat transfer measurement accuracy was practically independent of the Reynolds number and instead related simply to the protruding depth under different flow conditions. We correspondingly obtained a fitting correlation based on the calculation results $(q_w/q_0) = 1 + 0.68 \times L$ (with L in millimeters), which can be used to easily determine the influence of protruding installation on heat transfer measurement accuracy if the protruding length is known.

Next, marking a slight departure from the preceding pattern, we found that the effect of Reynolds number on q_w/q_0 was negligible only when L was less than 0.2 mm (Fig. 8b). For L values greater 0.2 mm, q_w/q_0 tended to vary as Reynolds number varied; the smaller the Reynolds number, the smaller the q_w/q_0 and the greater the impact on measurement accuracy. We investigated the temperature field and streamline around the sensor for different Reynolds numbers at recessed depth of 0.5 mm in effort to fully understand this difference, as shown in Fig. 9.

The recessed cavity flow, despite an extremely shallow cavity, proved to be much more complicated than the protruding

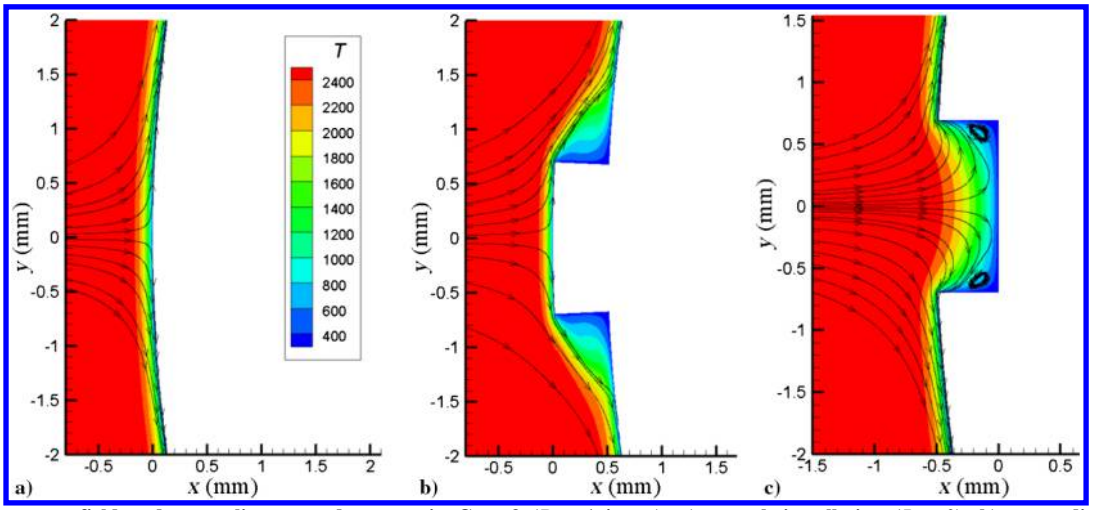

Fig. 6 Temperature field and streamline around sensors in Case 3 ($D = 1.4$ mm); a) smooth installation ($L = 0$); b) protruding installation ($L = 0.5$ mm); c) recessed installation ($L = 0.5$ mm).

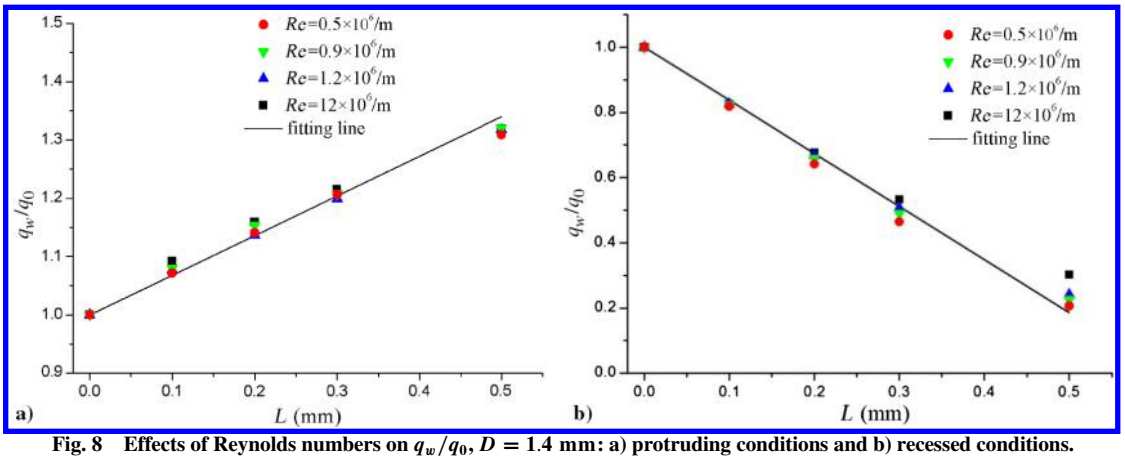

Fig. 8 Effects of Reynolds numbers on q_w/q_0, $D = 1.4$ mm: a) protruding conditions and b) recessed conditions.

cavity flow due to vortex structures formed at the surface of the sensors. The smaller the Reynolds number, the thicker the boundary layer and the bigger the vortex structures, which blocked the circular recessed cavity flow and decreased the velocity gradient, affecting heat flux measurement. When L is small, there is only a small vortex far from the sensitive element of the sensor and the velocity gradient is relatively free from disturbance, therefore, the Reynolds number has little effect on measurement accuracy at small recessed depths. The effect grows markedly at larger depths, however, due to the existence of larger vortexes in the cavity. Recall, though, that the recessed depth of actual unsmooth installation is usually very small, where the case of L close to 0.5 mm seldom exists. We accordingly wrote a fitting correlation between q_w/q_0 and recessed depth $(q_w/q_0) = 1–1.628L$ (again with L in millimeters), which can give an approximate evaluation of the effect of recessed installation on heat transfer measurement accuracy.

Because of the standard application of 1.4 mm coaxial thermocouples in our own laboratory, we focused specifically on evaluating 1.4 mm in sensors, though we also examined cases where D equaled 1.7 or 2 mm. Figures 10a and 9b show the influence of

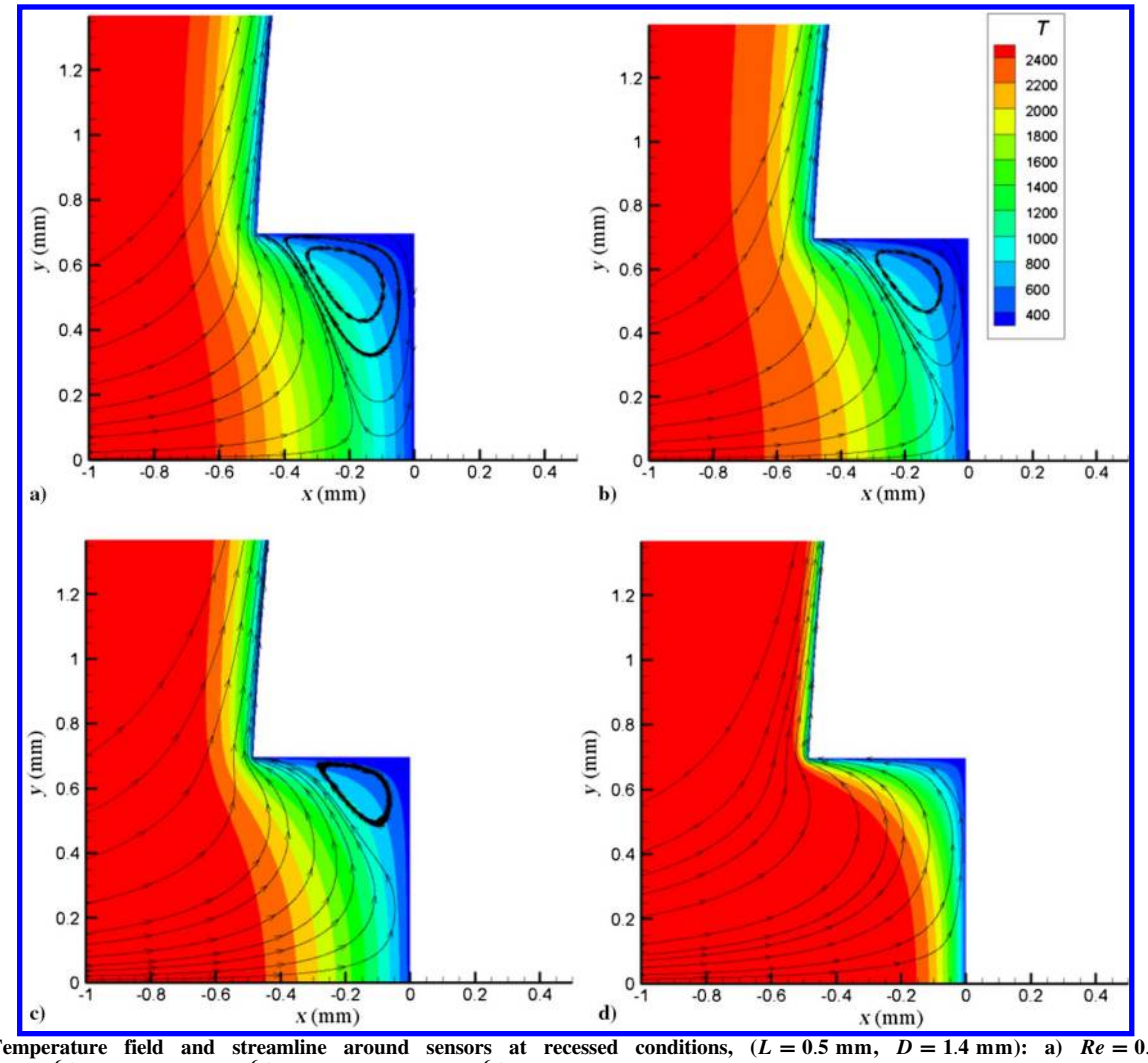

Fig. 9 Temperature field and streamline around sensors at recessed conditions, ($L = 0.5$ mm, $D = 1.4$ mm): a) $Re = 0.5 \times 10^6$/m, b) $Re = 0.9 \times 10^6$/m, c) $Re = 1.2 \times 10^6$/m, and d) $Re = 12 \times 10^6$/m.

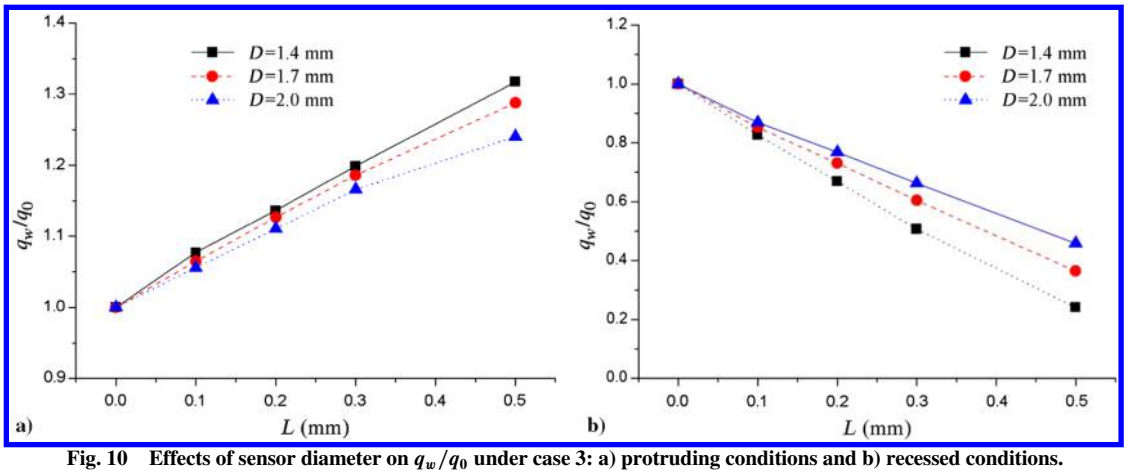

Fig. 10 Effects of sensor diameter on q_w/q_0 under case 3: a) protruding conditions and b) recessed conditions.

sensor diameter on q_w/q_0 with L from 0.1 to 0.5 mm under case 3 for protruding and recessed conditions, respectively. As shown in the figures, the value of q_w/q_0 on the depth varied approximately linearly compared with the different diameters we considered, but with differences in slope: The smaller the diameter, the larger the slope and the more severe the influence on measurement accuracy. This suggests that smaller diameter sensors should be especially carefully installed compared with larger sensors.

V. Conclusions

In this study, the influence of sensor installation on the accuracy of heat transfer measurement was examined, first through a series of experiments and then by simulating variable conditions and analyzing the relevant rules and mechanism of effects on the stagnation point. A few interesting conclusions were reached based on the numerical results obtained: First, protruding sensor installation results in larger deviation from actual heat transfer and recessed sensors result in smaller deviation compared with the results obtained with a smoothly installed sensor. Further, the larger the protruding/recessed depth, the more severe the deviation, and regardless of the Reynolds number, the level of deviation is basically proportional to the depth. Even recessed depth of only 0.1 mm causes results to be smaller by about 18%, and by 76% when it increases to 0.5 mm. The results are greater by about 8 and 32%, respectively, for protruding conditions at the same depths. These results suggest that special attention should be given to ensure that sensors are not installed in a recessed manner to prevent impact on heat transfer measurement accuracy. It was also found that different sensor diameters have differing influence on measurement accuracy; the smaller the diameter, the more severe the deviation. In short, thermal sensors absolutely must be installed as smoothly as possible with the model surface to ensure highly accurate heat transfer measurement.

Acknowledgments

This work was supported by the National Natural Science Foundation of China (Grants 11402275, 11472280, and 11532014).

References

[1] Wang, Q., Li, J. P., Zhao, W., and Jiang, Z. L., "Comparative Study on Aerodynamic Heating Under Perfect and Nonequilibrium Hypersonic Flows," *Science China Physics, Mechanics & Astronomy*, Vol. 59, No. 2, 2016, Paper 624701. doi:10.1007/s11433-015-5708-1

[2] Wu, S., Shu, Y. H., Li, J. P., and Yu, H. R., "An Integral Heat Flux Sensor with High Spatial and Temporal Resolutions," *Chinese Science Bulletin*, Vol. 59, No. 27, 2014, pp. 3484–3489. doi:10.1007/s11434-014-0464-6

[3] Gülhan, A., and Esser, B., "A Study on Heat Flux Measurements in High Enthalpy Flows," *35th AIAA Thermophysics Conference*, AIAA Paper 2001-3011, 2001. doi:10.2514/6.2001-3011

[4] Mazarakos, D. E., Sikoutris, D. E., Panagiotopoulos, E. E., Margaris, D. P., and Papanikas, D. G., "Stagnation Heat Transfer and Through-Thickness Temperature Profile Calculation and Hypersonic Speeds," *14th AIAA/AHI Space Planes and Hypersonic Systems and Technologies Conference*, AIAA Paper 2006-7939, 2006. doi:10.2514/6.2006-7939

[5] Mohammadiun, H., and Rahimi, A. B., "Stagnation-Point Flow and Heat Transfer of a Viscous, Compressible Fluid on a Cylinder," *Journal of Thermophysics and Heat Transfer*, Vol. 26, No. 3, 2012, pp. 494–502. doi:10.2514/1.T3833

[6] Xiong, Z. M., and Lele, S. K., "Simulation and Analysis of Stagnation Point Heat Transfer Under Free-Stream Turbulence," *41st Aerospace Sciences Meeting and Exhibit*, AIAA Paper 2003-1259, 2003. doi:10.2514/6.2003-1259

[7] Chadwick, K. M., "Stagnation Heat Transfer Measurement Techniques in Hypersonic Shock Tunnel Flows over Spherical Segments," *32nd Thermophysics Conference*, AIAA Paper 1997-2439, 1997. doi:10.2514/6.1997-2439

[8] Zeng, L., Gui, Y. W., Wang, A. L., Qin, F., and Zhang, H., "Study on Error Mechanism and Uncertainty Assessment of Heat Flux Measurement in Shock Tunnel," *Journal of Experiments in Fluid Mechanics*, Vol. 29, No. 5, 2015, pp. 15–25. doi:10.11729/syltlx20140135

[9] Coblish, J. J., Coulter, S. C., and Norris, J. D., "Aerothermal Measurement Improvements Using Coaxial Thermocouples at AEDC Hypervelocity Wind Tunnel No. 9," *45th AIAA Aerospace Sciences Meeting and Exhibit*, AIAA Paper 2007-1467, 2007. doi:10.2514/6.2007-1467

[10] Li, X. D., Hu, Z. M., and Jiang, Z. L., "Numerical Investigation on the Thermal Protection Mechanism for Blunt Body with Forward-Facing Cavity," *Science China Technological Sciences*, Vol. 59, No. 3, 2016, pp. 1–10. doi:10.1007/s11431-016-6015-4

[11] Kim, K. H., Kim, C., and Rho, O. H., "Methods for the Accurate Computations of Hypersonic Flows: I. AUSMPW + Scheme," *Journal of Computational Physics*, Vol. 174, No. 1, 2001, pp. 38–80. doi:10.1006/jcph.2001.6873

[12] Kitamura, K., Shima, E., Nakamura, Y., and Roe, P., "Evaluation of Euler Flux for Hypersonic Heating Computations," *AIAA Journal*, Vol. 48, No. 4, 2010, pp. 763–776. doi:10.2514/1.41605

[13] Jameson, A., and Yoon, S., "Lower-Upper Implicit Schemes with Multiple Grids for the Euler Equations," *AIAA Journal*, Vol. 25, No. 7, 1987, pp. 929–935. doi:10.2514/3.9724

[14] Fay, J., and Riddell, F., "Theory of Stagnation Point Heat Transfer in Dissociated Air," *Journal of the Aerospace Sciences*, Vol. 25, No. 2, 1958, pp. 73–85. doi:10.2514/8.7517

[15] Sun, Q. H., Zhu, H. Y., Wang, G., and Fan, J., "Effects of Mesh Resolution on Hypersonic Heating Prediction," *Theoretical and Applied Mechanics Letters*, Vol. 1, No. 2, 2011, pp. 37–40. doi:10.1063/2.1102201

This article has been cited by:

1. Lilei Hu, Andreas Mandelis, Zhenyu Yang, Xinxin Guo, Xinzheng Lan, Mengxia Liu, Grant Walters, Alexander Melnikov, Edward H. Sargent. 2017. Temperature- and ligand-dependent carrier transport dynamics in photovoltaic PbS colloidal quantum dot thin films using diffusion-wave methods. *Solar Energy Materials and Solar Cells* **164**, 135-145. [Crossref]